Revisiting the substitutional Mg acceptor binding energy of AlN

Ryota Ishii [1,*] Akira Yoshikawa [2] Mitsuru Funato [1] and Yoichi Kawakami [1]

[1]*Department of Electronic Science and Engineering, Kyoto University, Kyoto 615-8510, Japan*

[2]*Center for Integrated Research of Future Electronics, Institute of Materials Research and System for Sustainability,*
Nagoya University, Chikusa, Aichi 464-8601, Japan

Bipolar (*n*- and *p*-type) electric conductivity control is at the heart of semiconductor technologies. However, achieving such control in ultrawide-band-gap semiconductors has been a major challenge because of the very high donor and/or acceptor binding energies of these materials. In the case of aluminum nitride (AlN), which is an ultrawide-band-gap semiconductor and one of the first candidate materials for solid-state deep-ultraviolet emitters, the substitutional magnesium (Mg) acceptor binding energy has been reported to be at least 500 meV; thus, *p*-type electric conductivity control in AlN by Mg doping is believed to be unfeasible. Here, we experimentally and theoretically revisit the substitutional Mg acceptor binding energy of AlN. Our bound exciton luminescence and impurity-related transition spectroscopic studies indicate that the substitutional Mg acceptor binding energy of AlN is well below 500 meV. This statement is supported by variational calculations using anisotropic hole effective masses derived from first-principles calculations. The three independent approaches estimate the substitutional Mg acceptor binding energy of AlN to be 330 ± 80 meV. We find that considering electron-hole exchange interaction, hole anisotropy, and carrier-phonon coupling of AlN leads to a more realistic substitutional Mg acceptor binding energy.

I. INTRODUCTION

Bipolar (*n*- and *p*-type) electric conductivity control is at the heart of semiconductor technologies and has been a major challenge in the application of ultrawide-band-gap semiconductors [1] such as diamond [2], gallium oxide (α- and β-Ga_2O_3) [3], cubic and hexagonal boron nitride (*c*- and *h*-BN, respectively) [4–6], and aluminum nitride (AlN) [7]. Figure 1 shows the relationship between the room-temperature band gap E_g and the substitutional donor/acceptor binding energies of select wide-band-gap (4H-SiC and GaN) and ultrawide-band-gap semiconductors. The high *p*-type electric conductivity of diamond (e.g., a resistivity of 0.1 Ω cm by band conduction [23]) has been achieved by doping with B, whose acceptor binding energy is 370 meV. However, higher donor and/or acceptor binding energies of ultrawide-band-gap semiconductors impede control of the electric conductivity (*n*-type for diamond and *h*-BN, but *p*-type for Ga_2O_3 and AlN) and the subsequent realization of bipolar-conduction functional electronic and photonic devices.

To address or circumvent this issue, alternative concepts have been proposed, including field-emission devices [24], polarization doping [25], nanowires [26], tunnel junctions [27], and impurity-band (hopping) conduction [18,28]. Herein, we focus on photonic applications of ultrawide-band-gap semiconductors in the far-UVC spectral region (i.e., the wavelength range from 207 to 222 nm [29]) because far-UVC photons efficiently and safely inactivate influenza viruses [29] and human coronaviruses [30]. AlN and its related alloys are one of the first candidate materials for solid-state far-UVC emitters [31,32]. Although the aforementioned concepts will advance ultrawide-band-gap semiconductor science and technology, some shortcomings must first be addressed to enable the fabrication of bright far-UVC light emitters (e.g., parasitic photon absorption and the $3E_g$ rule [33]). Therefore we propose revisiting the potential of a classic approach: *p*-type electric conductivity control by magnesium (Mg) doping in AlN.

The substitutional Mg (Mg_{Al}) acceptor binding energy of AlN has been extensively studied by luminescence spectroscopy of bound excitons in conjunction with Haynes' rule [34,35], impurity-related transition spectroscopy [36], temperature-dependent Hall electrical measurements [7,19], effective-mass-approximation calculations [37], and first-principles calculations [38–40]. All of these previous studies have led to a consensus among researchers that the acceptor binding energy of Mg_{Al} is at least 500 meV in AlN and that *p*-type electric conductivity control in Mg-doped AlN is therefore unfeasible. However, we herein cast a doubt on the consensus because these previous works were conducted more than 10 years ago. Not only the crystalline quality but also the physical understanding of AlN has progressed dramatically over the past decade. In the present paper, we experimentally and theoretically revisit the Mg_{Al} acceptor binding energy of AlN and demonstrate that the binding energy is surprisingly smaller than commonly accepted, as shown in Fig. 1.

II. EXPERIMENTAL METHODS

We fabricated five metal–organic vapor phase epitaxy (MOVPE) grown homoepitaxial AlN films on *c*-plane AlN

*ryota.ishii@optomater.kuee.kyoto-u.ac.jp
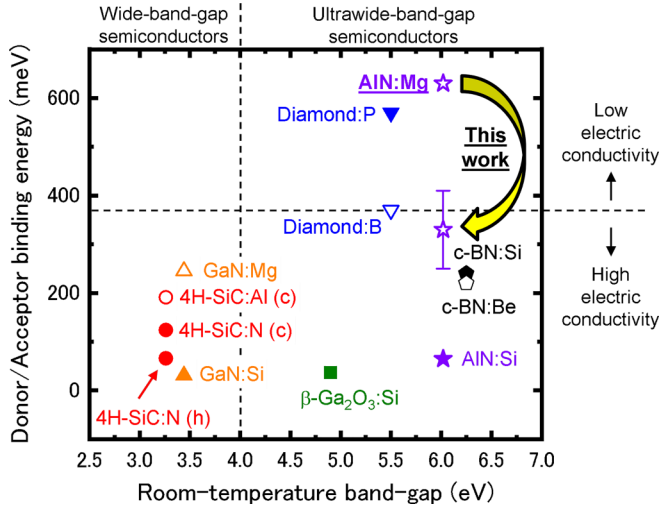
FIG. 1. Relation between the room-temperature band gap and substitutional donor/acceptor binding energies of select wide- and ultrawide-band-gap semiconductors (the values are tabulated in Table S1 in Ref. [8], Sec. 1). Closed and open symbols represent donor and acceptor cases, respectively. Low electric conductivity corresponds to the reported room-temperature resistivity of $\sim 10^6$ Ω cm (band conduction) for diamond:P [18] and $\sim 10^7$ Ω cm for AlN:Mg [19]. The reported acceptor binding energies of β-Ga$_2$O$_3$ are greater than 1 eV [20] (out of the range of Fig. 1). We did not plot the symbols for h-BN because of the controversy of the donor/acceptor binding energies [21,22].

substrates. The threading dislocation density of the substrate was on the order of 10^5 cm^{-2}. The MOVPE growth temperature was 1200 °C. A 1300-nm-thick undoped AlN layer was grown for the unintentionally doped AlN sample (UID). A 1-μm-thick Si-doped AlN layer was grown on a 300-nm-thick undoped AlN layer for the Si-doped AlN sample (Si#1), whereas a 1-μm-thick Mg-doped AlN layer was grown on a 2-μm-thick undoped AlN layer for the Mg-doped AlN samples. The Si concentration of the Si-doped AlN sample was 5×10^{16} cm^{-3}. Silane (SiH$_4$) was used for intentional Si doping. The Mg concentration of the three Mg-doped AlN samples was 5×10^{16} cm^{-3} (Mg#1), 4×10^{17} cm^{-3} (Mg#2), and 2×10^{18} cm^{-3} (Mg#3). Bis(cyclopentadienyl)magnesium (Cp$_2$Mg) was used for intentional Mg doping. All the samples were as-grown AlN (i.e., without activation-annealing). The impurity concentrations of the investigated samples, as determined by secondary ion mass spectrometry, are shown in Table I.

TABLE I. Impurity concentrations (cm^{-3}) of investigated AlN samples.

Sample name	[C]	[O]	[Si]	[Mg]
UID	$<2 \times 10^{16}$	$<1 \times 10^{16}$	$<3 \times 10^{15}$	not measured
Si#1	$<2 \times 10^{16}$	$<1 \times 10^{16}$	5×10^{16}	not measured
Mg#1	$<2 \times 10^{16}$	$<2 \times 10^{16}$	not measured	5×10^{16}
Mg#2	8×10^{16}	7×10^{16}	not measured	4×10^{17}
Mg#3	8×10^{16}	7×10^{16}	not measured	2×10^{18}
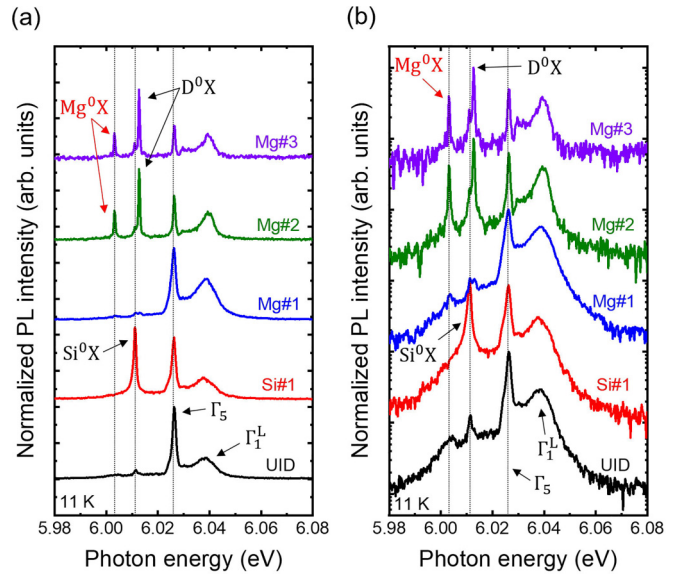
FIG. 2. (a) Linear and (b) logarithmic excitonic PL spectra of unintentionally doped (UID), Si-doped (Si#1), and Mg-doped (Mg#1, Mg#2, and Mg#3) AlN samples at 11 K. PL spectra are vertically shifted for clarity. The excitation power density is approximately 50 kW cm^{-2}. We set the free exciton (Γ_5) emission energy at 6.0262 eV to remove the effect of residual strain differences among the specimens. The raw PL spectra are depicted in Fig. S1 [8], Sec. 3. Strain-induced effects are detailed elsewhere [41,42].

Bound exciton (excitonic) and impurity-related transition photoluminescence (PL) spectroscopies were performed on the AlN specimens. The spectroscopic setup is detailed in Ref. [8], Sec. 2.

III. RESULTS AND DISCUSSION

A. Bound exciton luminescence spectroscopy

Figure 2 shows the excitonic PL spectra of UID, Si-doped (Si#1), and Mg-doped (Mg#1, Mg#2, and Mg#3) AlN specimens at 11 K. Previous studies have revealed that the 6.0262 eV (denoted as Γ_5) and 6.039 eV (denoted as Γ_1^L) peaks are free exciton emissions [43–47]. The 6.0110 eV peak (denoted as Si^{0}X) has been assigned as a neutral Si donor bound exciton transition [48,49]. We herein observe that the 6.0030 eV (denoted as Mg^{0}X) and 6.0126 eV (denoted as D^{0}X) peaks emerge with increasing Mg concentration in the Mg-doped AlN samples.

The 6.0030 eV peak has two possible origins: neutral or ionized Mg acceptor bound exciton transitions. We conclude that the latter bound exciton transition is unlikely given the effective mass imbalance of electrons and holes in AlN [50], which is similar to that in GaN (a member of the same material family as AlN) [51]. Therefore we assign the 6.0030 eV peak as a *neutral* Mg acceptor bound exciton emission (Mg^{0}X). This assignment is supported by the optical polarization analysis in Fig. S2 [8], Sec. 3. Meanwhile, given the photon energy of the D^{0}X peak, it should be attributed to a *donor* bound exciton transition involved in Mg incorporation (temperature-dependent excitonic PL spectra are shown in Fig. S3 [8],
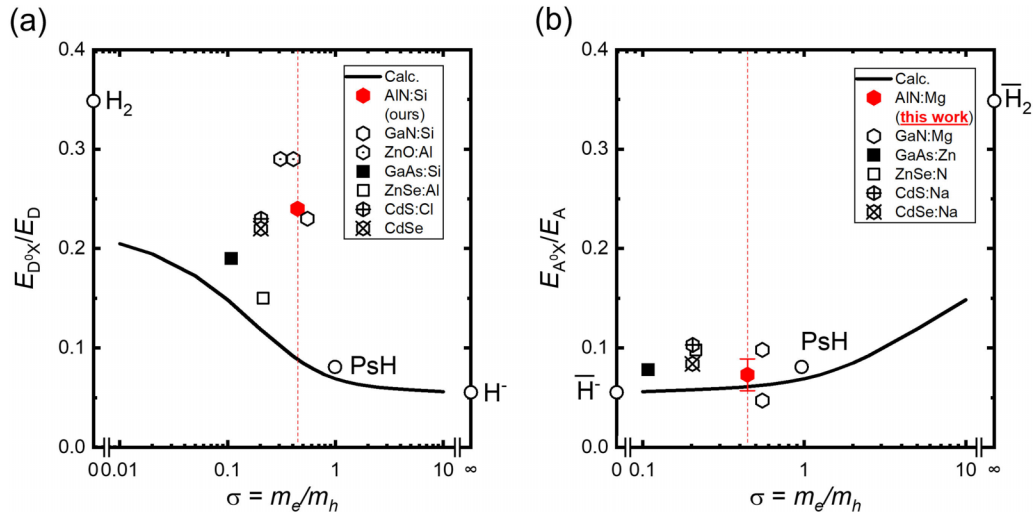
FIG. 3. Effective mass ratio ($\sigma = m_e/m_h$) dependence of (a) E_{D^0X}/E_D and (b) E_{A^0X}/E_A for select III–V and II–VI compound semiconductors. m_e and m_h are the effective masses of an electron and a hole, respectively. E_{D^0X} and E_{A^0X} are the binding energy of a neutral donor and acceptor bound exciton, respectively. E_D and E_A are the binding energy of a donor and an acceptor, respectively. The electron (hole) effective masses in anisotropic materials are averaged by the harmonic mean as $1/m_{e(h)} = 1/3 \times (2/m_{e(h),\perp} + 1/m_{e(h),\parallel})$, where $m_{e(h),\parallel}$ and $m_{e(h),\perp}$ are the electron (hole) effective masses parallel and perpendicular to the c axis, respectively. The material parameters are tabulated in Tables S2 and S3 in Ref. [8], Sec. 5. The estimated σ of AlN (0.45) is depicted by a red dotted line. H_2, PsH, and H^- are the hydrogen molecule, positronium hydride, and hydride anion, respectively [49]. $\overline{H}_2$ and $\overline{H}^-$ are the antimatter of the hydrogen molecule and hydride anion, respectively. The black solid curve represents the theoretical result reproduced from a numeric table [54]. The red hexagon with an error bar (AlN:Mg) is generated from the results of Figs. 2 and 7.

Sec. 4.). Although hydrogen- [52] or nitrogen-vacancy-related [51] *donor* bound exciton emissions are a plausible origin of the D^0X peak, further assignment is beyond the scope of the present paper. Below, we focus on the *acceptor* physics of AlN.

Comparing the energy difference between the Mg^0X and Γ_5 peaks reveals that the neutral Mg acceptor bound exciton binding energy is 23.2 meV. Surprisingly, our estimated value is approximately one-half of the previously estimated one (40 meV) [34]. The misinterpretation in previous studies likely originated from the relatively broad luminescence linewidth of the samples resulting from their heteroepitaxial growth [34]. In addition, from a physical viewpoint, previous studies overlooked the Γ_5 free exciton emission and did not notice the huge electron-hole exchange interaction in AlN, which was first reported in 2013 [44].

There is a well-known empirical rule (Haynes' rule [35]) in semiconductor physics that the acceptor (donor) binding energy E_A (E_D) is related to the neutral acceptor (donor) bound-exciton binding energy E_{A^0X} (E_{D^0X}) [53]. The energy ratio E_{A^0X}/E_A (E_{D^0X}/E_D) is related to the effective mass ratio $\sigma = m_e/m_h$ within the effective mass approximation [54], where m_e and m_h are the effective masses of electrons and holes, respectively. The relation is depicted for select III–V and II–VI compound semiconductors for donor [Fig. 3(a)] and acceptor [Fig. 3(b)] cases. In direct-band-gap semiconductors, m_h is typically greater than m_e; thus, σ ranges from 0.1 to 1 among the materials. Contrary to the donor case [Fig. 3(a)], $E_{A^0X}/E_A \sim 0.09$ empirically holds for most of the materials [Fig. 3(b)]. This behavior can be qualitatively understood on the basis of the theoretical curve in Fig. 3(b), which shows that E_{A^0X}/E_A is almost independent of σ in the range $0.1 \leqslant \sigma \leqslant 1$

[54]. Because AlN has a σ of 0.45, we may expect that the same empirical rule holds for AlN, leading to a Mg acceptor binding energy of 258 meV. Meanwhile, the theoretical curve [54] in Fig. 3(b) estimates the Mg acceptor binding energy of AlN to be 390 meV. In either case, our bound-exciton luminescence study indicates that the substitutional Mg acceptor binding energy of AlN is substantially smaller than the commonly accepted binding energy of at least 500 meV [7,19,34,36–40]. In short, our bound exciton luminescence spectroscopic study suggests that the substitutional Mg acceptor binding energy of AlN is in the range 258–390 meV.

B. Impurity-related transition spectroscopy

Because our bound-exciton luminescence study indicated that the substitutional Mg acceptor binding energy of AlN is shallower than believed, we next revisited the impurity-related transitions using steady and time-resolved PL spectroscopies. Figure 4 shows the impurity-related transition PL spectra of UID, Si-doped, and Mg-doped AlN samples at 11 K. The 5.5 eV band emission appears with increasing Mg concentration, indicating that the emission peak is related to Mg. This emission band has also been observed in previous studies, where it was assigned as a donor-acceptor pair (DAP) recombination band involving a Mg acceptor and a shallow donor [26,36]. Under the assumption of a shallow donor binding energy of 60 meV, one of the previous studies estimated the substitutional Mg acceptor binding energy of AlN to be 510 meV [36]. However, we note that DAP emission bands generally have two characteristic features: a red-shift of the emission with increasing time delay and a blue-shift of the emission with increasing excitation intensity [50]. Figures 5(a)–5(c) show the streak-camera image, time-evolution,
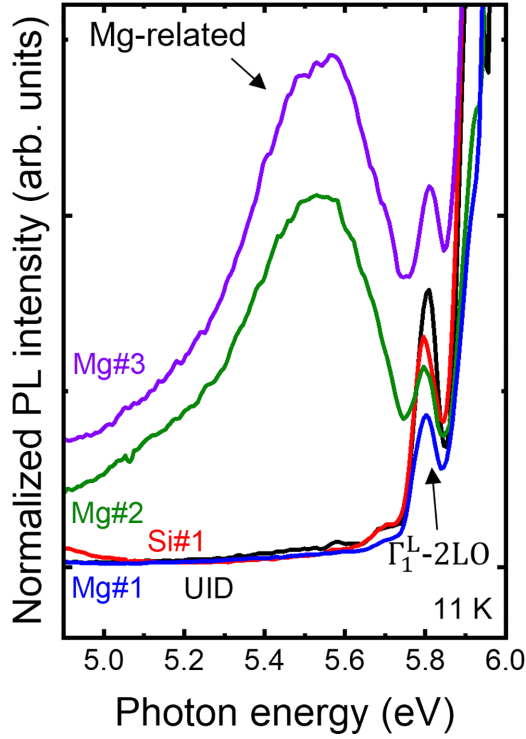
FIG. 4. Impurity-related transition PL spectra of UID, Si-doped (Si#1), and Mg-doped (Mg#1, Mg#2, and Mg#3) AlN samples at 11 K. The PL intensities are normalized by the peak intensity of the free exciton emission around 6 eV. The excitation power density is approximately 125 kW cm^{-2}.

and temporal response of the 5.5 eV band emission, respectively, for a Mg-doped AlN sample (Mg#3) at 11 K. Neither a red-shift nor a blue-shift of the 5.5 eV band is observed, indicating that the 5.5 eV band emission is unlikely to be a DAP recombination. This interpretation is reinforced by additional experimental results in Figs. S5 and S6 in Ref. [8], Sec. 6.

Consequently, we assign the 5.5 eV band emission as a recombination of a free electron with a neutral Mg acceptor (e–Mg^0). Note that a previous first-principles calculation study has suggested that the e–Mg^0 emission peak should appear at 4.77 eV, while the 5.5 eV band emission should originate from a recombination of an electron with a hole in Mg$_{Al}^+$ state [40]. However, we did not observe an emission peak at 4.77 eV from Mg-doped AlN samples as shown in Figs. 6 and S7 in Ref. [8], Sec. 7. In addition, the Mg$_{Al}^+$ state should be found only in highly p-type conductive AlN in the spirit of Ref. [40]. Our as-grown Mg-doped AlN samples are, however, highly resistive. Therefore we do not support the interpretation of Ref. [40]. The discrepancy of acceptor physics between first-principles calculations and experiments has also been reported in GaN [40,65–67].

To gain insight into the physics of the 5.5 eV band emission, we conducted temperature-dependent PL spectroscopy using a high-repetition-rate laser that enabled us to acquire the 5.5 eV band emission with a high signal-to-noise ratio at room temperature under weak excitation conditions. Figure 6(a) shows the experimental (black solid line) PL

spectrum of a Mg-doped AlN sample (Mg#3) at 11 K. A Gaussian function-fitted spectrum (fitted using high-energy side of the 5.5 eV band emission) in Fig. 6(a) indicates that the 5.5 eV band emission has an asymmetric spectral shape (i.e., a low-energy tail). In addition, the 5.5 eV band emission shows a huge spectral linewidth compared with the thermal broadening energy. These behaviors suggest the non-negligible carrier–phonon coupling. Within the one-dimensional configuration-coordinate (1D cc) diagram approximation, the luminescence spectral shape $I(E)$ at cryogenic temperatures and the temperature dependence of the full width at half maximum (FWHM) $W(T)$ of defects are expressed as [51,68,69]

$$I(E) = \sum_n e^{-S} \frac{(S)^n}{n!} \times \frac{I}{w\sqrt{\pi/2}}$$
$$\times \exp\left(\frac{-2(E_{ZPL} - n\hbar\omega_{gr} - E)^2}{w^2}\right), \qquad (1)$$

$$W(T) = W(0)\sqrt{\coth\left(\frac{\hbar\omega_{ex}}{2kT}\right)}, \qquad (2)$$

where S is the Huang–Rhys factor. $\hbar\omega_{gr}$ and $\hbar\omega_{ex}$ are the averaged vibration energy of the ground and excited states, respectively. E_{ZPL} is the zero-phonon (vibration) energy, and n is a positive integer. Parameters I and w describe the intensity and linewidth of the Gaussian function, respectively, and k is the Boltzmann constant. The PL spectrum fitted using Eq. (1) is depicted in Fig. 6(a) (red dotted line). Contrary to the Gaussian function fitting, this fitting reproduces the asymmetric experimental PL spectral shape. Although we could not uniquely determine the fitting parameters in Eq. (1) (detailed in Fig. S7 in Ref. [8], Sec. 7), we could estimate the ranges as $S = 2.8$–4.2, $\hbar\omega_{ex} = 60$–110 meV, and $E_{ZPL} = 5.69$–5.84 eV. Figure 6(b) shows the temperature dependence of the FWHM of the 5.5 eV band emission and the fitted result using Eq. (2). The estimated $\hbar\omega_{ex}$ is 31 meV. Our estimated vibration energies of Mg$_{Al}$ in AlN are comparable to those of GaN [70–72]. Following these fitting results, we depicted the 1D cc diagram of Mg$_{Al}$ in Fig. 7. This diagram indicates that the energy difference between the e–Mg^0 recombination peak (5.55 eV) and band gap (6.1 eV) does not correspond to the acceptor binding energy as previously suggested [26,36]. Instead, the energy difference between E_{ZPL} and band gap gives a true acceptor binding (thermal activation) energy of Mg$_{Al}$ in AlN.

In summary, our impurity-related transition spectroscopic study suggests that the substitutional Mg acceptor binding energy of AlN is in the range 260–410 meV. Again, our extracted Mg acceptor binding energy of AlN is substantially smaller than the accepted value of at least 500 meV [7,19,34,36–40]. At this stage, we independently determined the E_A (from Fig. 7) and E_{A^0X} (from Fig. 2) of AlN:Mg. The ratio with an error bar is plotted as a function of σ in Fig. 3(b). Our experimentally extracted ratio is in good agreement with the theoretically predicted [54] and empirical ($E_{A^0X}/E_A \sim 0.09$) values.
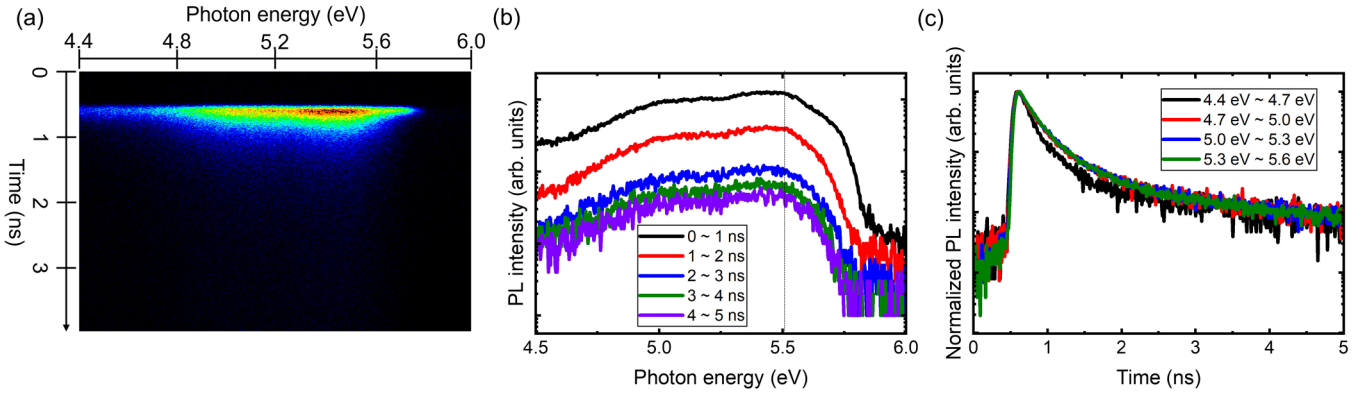
FIG. 5. (a) Streak-camera image, (b) time-evolution, and (c) temporal response of the 5.5 eV band emission for a Mg-doped sample with the Mg concentration of 2×10^{18} cm^{-3} (Mg#3) at 11 K. The peak excitation power density is approximately 580 MW cm^{-2}. The time and spectral integration ranges are written in Figs. 5(b) and 5(c), respectively.

C. Hole anisotropy

To theoretically interpret our experimental results, we examined the Mg$_{Al}$ acceptor binding energy of AlN within the effective mass approximation. The Hamiltonian of a hole bound by an acceptor in wurtzite crystals can be written as

$$H = -\frac{\hbar^2}{2}\left[\frac{1}{m_h^\perp}\left(\frac{\partial^2}{\partial x^2}+\frac{\partial^2}{\partial y^2}\right)+\frac{1}{m_h^\parallel}\frac{\partial^2}{\partial z^2}\right]$$
$$-\frac{e^2}{4\pi}\frac{1}{\sqrt{\epsilon^\perp\epsilon^\parallel(x^2+y^2)+(\epsilon^\perp)^2 z^2}}, \quad (3)$$
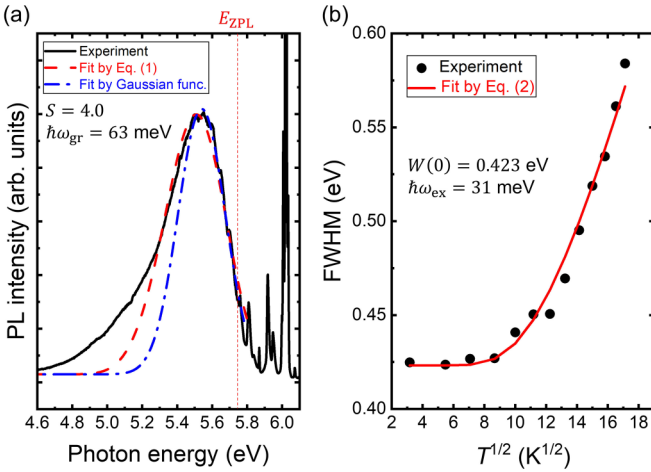
FIG. 6. (a) Experimental and fitted PL spectra of the Mg-related transition for a Mg-doped AlN sample (Mg#3) at 11 K. The peak excitation power density is approximately 21 kW cm^{-2}. As we could not uniquely determine the fitting parameters in Eq. (1), an example of the fitted result using Eq. (1) is shown. Note that the low-energy tail and peak energy of the experimental PL spectrum could not be reproduced well using Eq. (1) with any fitting parameter set, likely because of the limitation of the one-dimensional configuration-coordinate diagram approximation under weak/moderate carrier–phonon coupling conditions as suggested in a previous study [68]. (b) Temperature dependence of the full width at half maximum (FWHM) of the 5.5 eV band emission.

where $\hbar$ and e are the Dirac constant and elementary charge, respectively. $\epsilon^\parallel$ and $\epsilon^\perp$ are the static dielectric constant parallel and perpendicular to the c axis of wurtzite crystals, respectively, and $m_h^\parallel$ and $m_h^\perp$ are the hole effective masses parallel and perpendicular to the c axis of wurtzite crystals, respectively. With the variable change $(x, y, z) = (x', y', \sqrt{m^\parallel/m^\perp}z')$, Eq. (3) can be rewritten as

$$H = H_0 + H_1, \quad (4)$$

$$H_0 = -\frac{\hbar^2}{2m_h^\perp}\left(\frac{\partial^2}{\partial x'^2}+\frac{\partial^2}{\partial y'^2}+\frac{\partial^2}{\partial z'^2}\right)$$
$$-\frac{e^2}{4\pi\sqrt{\epsilon^\parallel\epsilon^\perp}}\frac{1}{\sqrt{x'^2+y'^2+z'^2}}, \quad (5)$$

$$H_1 = \frac{e^2}{4\pi\sqrt{\epsilon^\parallel\epsilon^\perp}}\left(\frac{1}{\sqrt{x'^2+y'^2+z'^2}}-\frac{1}{\sqrt{x'^2+y'^2+Az'^2}}\right), \quad (6)$$

where A is the anisotropic parameter defined as $A = (m_h^\perp\epsilon^\perp)/(m_h^\parallel\epsilon^\parallel)$. Equation (5) is nothing but the hydrogen-atom problem in a new coordinate system (x', y', z') with an average dielectric constant of $\sqrt{\epsilon^\parallel\epsilon^\perp}$ and a hole effective mass of $m_h^\perp$. That is, a hole bound problem in wurtzite crystals can be reasonably reduced to the hydrogen-atom problem if $A \sim 1$. Using this hypothesis, Taniyasu et al. have linked their experimentally deduced Mg acceptor binding energy (630 meV) of AlN to the hole effective mass ($3.3m_0$, where m_0 is the electron mass in vacuum) [7]. Nam et al. have also estimated the hole effective mass of AlN to be $2.7m_0$ in a similar manner [36]. Using an isotropic impurity pseudopotential, a previous effective-mass calculation study deduced a substitutional Mg acceptor binding energy of 514–789 meV for AlN [37].

Can the effect of hole anisotropy be ignored for AlN? To answer this question, we calculated the electronic band structure of AlN by first-principles calculations, see Refs. [73,74] and [8, Sec. 8]. Figure 8(a) shows the crystal structure (wurtzite structure) of AlN. Electrons and holes in wurtzite crystals are generally anisotropic because of their uniaxial nature. Figure 8(b) shows the calculated electronic band structure of AlN. The estimated band gap is 4.05 eV. Although the estimated band gap is considerably smaller than the
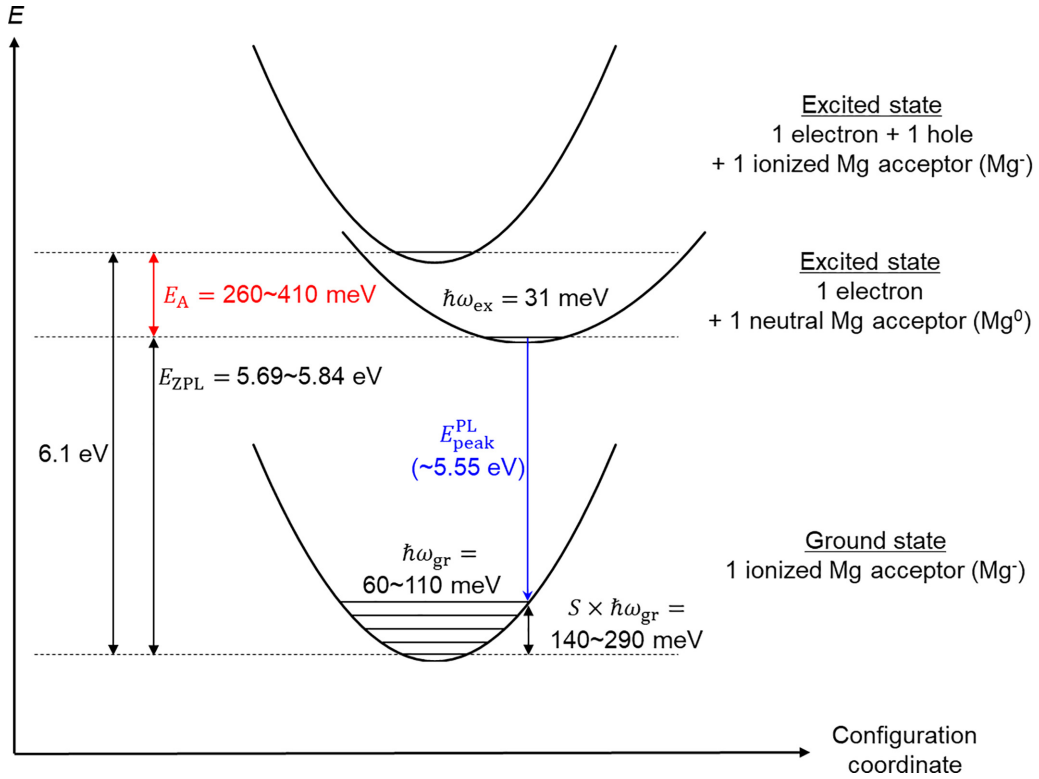
FIG. 7. One-dimensional configuration-coordinate diagram of Mg_{Al} in AlN. We assigned the 5.5 eV band emission (blue downward arrow in the figure) as a recombination of a free electron with a neutral Mg acceptor (electron $+ Mg^0 \rightarrow Mg^- +$ photon).

experimental one, the valence-band structure is reproduced well [78]. In fact, the energy difference [Δ in Fig. 8(c)] between the crystal-field split-off hole (CH) and heavy hole (HH) bands at the Γ point agrees well with the experimental one [42], confirming the reliability of our calculated valence-band structure. Figure 8(c) shows the expanded electronic band structure of AlN at the valence-band maximum (the region of interest in this study). To investigate the hole bound problem, the topmost valence band (CH band in this case) must be considered. In the case of (unstrained) AlN, the contribution from the HH and light hole (LH) bands can be safely ignored because of the large Δ. Figure 8(c) clearly shows that the CH band of AlN has huge anisotropy that is quantitatively characterized by the hole effective masses ($m^{\parallel}_{CH}$ and $m^{\perp}_{CH}$) given in Table II. Both the previous and our first-principles

calculation results tabulated in Table II show the huge anisotropy of the CH band of AlN. These theoretical considerations indicate that the effect of hole anisotropy should not be neglected for the acceptor bound hole problem of AlN.

D. Acceptor binding energy calculated by perturbation and variational methods

To evaluate the effect of hole anisotropy, we numerically solved Eq. (4) using perturbation [79] and variational [80] methods. Figure 8(d) shows the effect of hole anisotropy on the acceptor energy ($-E_A$). The variational calculation result should be more plausible because the exact energy is lower than the calculated energy. Because the A value for AlN is 10–13 (Table II), the hole anisotropy substantially reduces the

TABLE II. Effective masses of crystal-field split-off hole and anisotropic parameter of AlN. $m^{\parallel}_{CH}$ and $m^{\perp}_{CH}$ are the crystal-field split-off hole effective masses parallel and perpendicular to the c axis, respectively. A is the anisotropic parameter defined by $A = (m^{\perp}_{CH}\epsilon^{\perp}_0)/(m^{\parallel}_{CH}\epsilon^{\parallel}_0)$, where $\epsilon^{\parallel}$ and $\epsilon^{\perp}$ are the static dielectric constant parallel and perpendicular to the c axis, respectively. $m^{\parallel,*}_{CH}$, $m^{\perp,*}_{CH}$, and A^* are the polaron-corrected effective masses and anisotropic parameter, respectively. We used experimentally obtained static dielectric constants as $\epsilon^{\parallel}_0 = 9.21\epsilon_0$ and $\epsilon^{\perp}_0 = 7.65\epsilon_0$ [81]. The assumed longitudinal optical phonon energy of AlN is 110 meV. Abbreviations are defined as follows: PAWPP: projector-augmented wave pseudopotential, PBE: Perdew–Burke–Ernzerhof, FP-LMTO: full-potential linearized muffin-tin orbital, LDA: local density approximation, NCPP: norm-conserving pseudopotential, QSGW: quasiparticle self-consistent GW.

Reference	$m^{\parallel}_{CH}$ ($m^{\parallel,*}_{CH}$)	$m^{\perp}_{CH}$ ($m^{\perp,*}_{CH}$)	A (A^*)	Notes
This work	0.29 (0.33)	4.04 (6.40)	11.6 (16.3)	PAWPP, PBE
Kim *et al.* [55,82]	0.26 (0.29)	4.05 (6.42)	12.9 (18.3)	FP-LMTO, LDA
Yan *et al.* [56][a]	0.25 (0.28)	3.20 (4.81)	10.6 (14.3)	NCPP, G_0W_0
Punya and Lambrecht [83]	0.25 (0.28)	3.53 (5.42)	11.7 (16.1)	FP-LMTO, QSGW

[a]We converted the reported Luttinger-like parameters to the hole effective masses by calculating the valence-band energy dispersion of AlN.
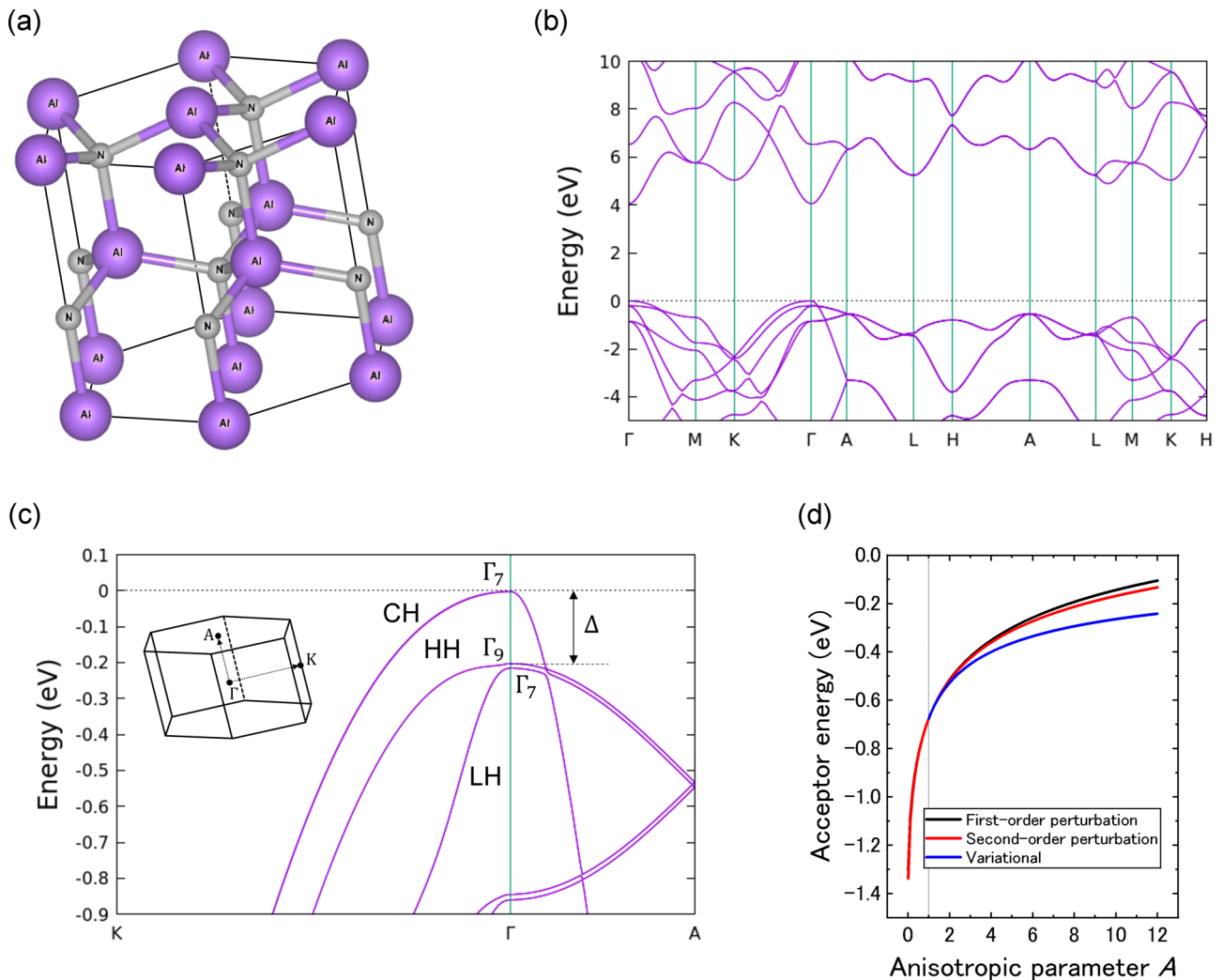
FIG. 8. (a) Crystal structure (wurtzite structure) [77], (b) electronic band structure, and (c) expanded electronic band structure at the valence-band maximum of AlN. The inset in (c) represents the first Brillouin zone of wurtzite crystals. CH, HH, and LH denote the crystal-field split-off hole, heavy hole, and light hole bands, respectively. (d) Anisotropic parameter dependence of the acceptor energy ($-E_A$) calculated by perturbation [79] and variational [80] methods. The material parameters used are $m_h^\perp = 3.5m_0$, $\epsilon^\parallel = 9.21\epsilon_0$, and $\epsilon^\perp = 7.65\epsilon_0$ [81], where ϵ_0 is the vacuum permittivity.

acceptor binding energy. Our variational calculations estimate the acceptor binding energy of AlN to be 284, 270, 235, and 247 meV, when using the effective masses reported in this work and those reported by Kim *et al.* [55,82], Yan *et al.* [56], and Punya and Lambrecht [83], respectively (Table II). All of the calculated energies are well below the commonly accepted Mg acceptor binding energy and our experimentally deduced values. Here, we must recall the non-negligible carrier–phonon coupling in AlN [45]. In case of polar materials, polaron correction must be considered [84,85]. The polaron correction generally increases the acceptor binding energy of semiconductors. The polaron-corrected hole effective masses of AlN are derived using the mass enhancement factor in Ref. [89]. Table II shows the polaron-corrected hole effective masses ($m_{CH}^{\parallel,*}$ and $m_{CH}^{\perp,*}$) and anisotropic parameter (A^*) for AlN. Our variational calculations estimate the acceptor binding energy of AlN to be 379, 358, 305, and 323 meV, using the poralon-corrected hole effective masses reported in the present work and those reported by Kim *et al.* [55,82],

Yan *et al.* [56], and Punya and Lambrecht [83], respectively (Table II). The calculated acceptor binding energies of AlN are in good agreement with our experimental results but disagree with previously reported experimental values (500 meV or greater) [7,19,34,36].

To summarize, our variational calculation suggests that the substitutional Mg acceptor binding energy of AlN is in the range 305–379 meV. Note that the chemical shift or central-cell correction is not considered in this manuscript. We assume that these effects play a minor role because Mg is an isocoric impurity of Al [86].

E. Discussion on previous first-principles calculations and electrical characterizations

Finally, we discuss previously reported results of first-principles calculations and electrical characterizations. Using first-principles calculations, other authors have estimated the substitutional Mg acceptor binding energy of AlN to be in the

range 500–780 meV [38–40]. The reported values are scattered. One group has reported that Be is a better dopant than Mg for *p*-type doping in AlN [38], whereas another group has recommended Mg [39]. Some groups have insisted that Mg is an effective mass acceptor in AlN [39,87], while another group has suggested that Mg is not an effective mass acceptor [40]. Therefore we can at least argue that first-principles calculation studies have not led to a solid conclusion about the acceptor physics of AlN. This situation is also true for GaN [40,65–67] as we already mentioned. In the present paper, we found that hole anisotropy strongly influences the acceptor binding energy of AlN. Therefore we propose that the effect of hole anisotropy should be explicitly considered in future first-principles calculation studies. The tuning condition of hybrid functional should be also examined as suggested in a previous study for GaN [67].

With respect to temperature-dependent Hall electrical measurements, previous studies have estimated the Mg acceptor binding energy of AlN to be 630 meV [7] or 500 meV [19]. These values are higher than those of the binding energies we determined. We attribute this difference to the formation of a deeper state, such as DX (AX) centers or dual acceptor states [88] (not depicted in Fig. 7). That is, the excited state [1 electron + 1 neutral Mg acceptor (Mg^0)] in Fig. 7 is a metastable state. We want to emphasize that, electrical characterizations are likely to probe the most stable state, whereas optical spectroscopic characterizations can also investigate metastable states. For Si-doped AlN, a previous electrical characterization study estimated the Si donor binding energy to be 282 meV [7]. However, in a later electrical characterization study, the binding energy was revised to 70 meV using Si-implanted and non-equilibrium-annealed AlN samples [89,90]. By contrast, optical spectroscopic characterizations have estimated the Si donor binding energy to be ∼70 meV from the outset (using Si-doped AlN samples with no special treatments) [48,49]. Therefore optical spectroscopic approaches are intrinsically superior for investigating

both the stable and metastable impurity-related electronic states. Nevertheless, with respect to practical applications, donor and acceptor binding energies must be shallow in terms of electrical characterizations. Special treatments to eliminate deeper states in AlN:Mg should be explored, like *n*-type AlN [89,90]. We propose that eliminating the D^0X peak in Fig. 2 and the 4.4 eV band in Fig. S7(a) should be one of the guidelines for obtaining high *p*-type electric conductivity in Mg-doped AlN because these origins should correspond to a compensating center.

IV. CONCLUSION

In conclusion, we experimentally and theoretically revisited a substitutional Mg acceptor binding energy of AlN. The three independent approaches indicate that the binding energy is substantially shallower than believed. We estimated the substitutional Mg acceptor binding energy of AlN as 330 ± 80 meV, as an averaged value of the three approaches. Previous studies have overlooked the electron–hole exchange interaction, hole anisotropy, and carrier–phonon coupling in AlN, leading to misinterpretations that the substitutional Mg acceptor binding energy is 500 meV or greater. Figure 1 suggests that *p*-type electric conductivity control by Mg doping in AlN is feasible. A simple Boltzmann statistical analysis $\exp(-330/26)/\exp(-630/26)$ (compared with a previous Mg acceptor binding energy [7]) indicates that the room-temperature hole density can be more than 10000 times greater than previously believed. We hope our findings will stimulate further experimental and theoretical studies on the impurity bound problems and bipolar conductivity control in ultrawide-band-gap semiconductors.

[1] J. Y. Tsao, S. Chowdhury, M. A. Hollis, D. Jena, N. M. Johnson, K. A. Jones, R. J. Kaplar, S. Rajan, C. G. Van de Walle, E. Bellotti, C. L. Chua, R. Collazo, M. E. Coltrin, J. A. Cooper, K. R. Evans, S. Graham, T. A. Grotjohn, E. R. Heller, M. Higashiwaki, M. S. Islam, P. W. Juodawlkis *et al.*, Adv. Electron. Mater. **4**, 1600501 (2018).

[2] S. Koizumi, K. Watanabe, M. Hasegawa, and H. Kanda, Science **292**, 1899 (2001).

[3] M. Higashiwaki, K. Sasaki, A. Kuramata, T. Masui, and S. Yamakoshi, Appl. Phys. Lett. **100**, 013504 (2012).

[4] O. Mishima, J. Tanaka, S. Yamaoka, and O. Fukunaga, Science **238**, 181 (1987).

[5] K. Watanabe, T. Taniguchi, and H. Kanda, Nat. Mater. **3**, 404 (2004).

[6] G. Cassabois, P. Valvin, and B. Gil, Nat. Photonics **10**, 262 (2016).

[7] Y. Taniyasu, M. Kasu, and T. Makimoto, Nature (London) **441**, 325 (2006).

[8] See Supplemental Material at http://link.aps.org/supplemental/10.1103/PhysRevB.108.035205 for (Sec. 1) reported room-

temperature band gap and donor/acceptor binding energies of select wide- and ultrawide-band-gap semiconductors, which includes Refs. [9–17]; (Sec. 2–4) spectroscopic setup, raw and polarization-resolved excitonic PL spectra, and temperature-dependent excitonic PL spectra; (Sec. 5) effective masses and binding energies of select III-V and II-VI compound semiconductors, which includes Refs. [57–65]; (Sec. 6,7) the assignment of the 5.5 eV band emission and one dimensional configuration-coordinate diagram analysis, which includes a Ref. [67]; and (Sec. 8) the calculation details of first-principles calculations, which includes Refs. [75,76].

[9] H. Matsunami, Proc. Jpn. Acad., Ser. B **96**, 235 (2020).

[10] M. Ikeda, H. Matsunami, and T. Tanaka, Phys. Rev. B **22**, 2842 (1980).

[11] O. Madelung, *Semiconductors: Data Handbook* (Springer, Berlin, 2004).

[12] H. Wang and A.-B. Chen, J. Appl. Phys. **87**, 7859 (2000).

[13] S. Brochen, J. Brault, S. Chenot, A. Dussaigne, M. Leroux, and B. Damilano, Appl. Phys. Lett. **103**, 032102 (2013).

[14] K. Irmscher, Z. Galazka, M. Pietsch, R. Uecker, and R. Fornari, J. Appl. Phys. **110**, 063720 (2011).

[15] H. Kato, M. Ogura, T. Makino, D. Takeuchi, and S. Yamasaki, Appl. Phys. Lett. **109**, 142102 (2016).

[16] K. Hirama, Y. Taniyasu, H. Yamamoto, and K. Kumakura, Appl. Phys. Lett. **116**, 162104 (2020).

[17] T. Taniguchi, S. Koizumi, K. Watanabe, I. Sakaguchi, T. Sekiguchi, and S. Yamaoka, Diam. Relat. Mater. **12**, 1098 (2003).

[18] S. Yamasaki, E. Gheeraert, and Y. Koide, MRS Bull. **39**, 499 (2014).

[19] M. L. Nakarmi, N. Nepal, C. Ugolini, T. M. Altahtamouni, J. Y. Lin, and H. X. Jiang, Appl. Phys. Lett. **89**, 152120 (2006).

[20] M. J. Tadjer, J. L. Lyons, N. Nepal, J. A. Freitas Jr., A. D. Koehler, and G. M. Foster, ECS J. Solid State Sci. Technol. **8**, Q3187 (2019).

[21] R. J. P. Román, F. J. R. C. Costa, A. Zobelli, C. Elias, P. Valvin, G. Cassabois, B. Gil, A. Summerfield, T. S. Cheng, C. J. Mellor, P. H. Beton, S. V. Novikov, and L. F. Zagonel, 2D Mater. **8**, 044001 (2021).

[22] S. Lu, P. Shen, H. Zhang, G. Liu, B. Guo, Y. Cai, H. Chen, F. Xu, T. Zheng, F. Xu, X. Chen, D. Cai, and J. Kang, Nat. Commun. **13**, 3109 (2022).

[23] J. Barjon, N. Habka, C. Mer, F. Jomard, J. Chevallier, and P. Bergonzo, phys. stat. sol. (RRL) **3**, 202 (2009).

[24] K. Watanabe, T. Taniguchi, T. Niiyama, K. Miya, and M. Taniguchi, Nat. Photonics **3**, 591 (2009).

[25] J. Simon, V. Protasenko, C. Lian, H. Xing, and D. Jena, Science **327**, 60 (2010).

[26] S. Zhao, A. T. Connie, M. H. T. Dastjerdi, X. H. Kong, Q. Wang, M. Djavid, S. Sadaf, X. D. Liu, I. Shih, H. Guo, and Z. Mi, Sci. Rep. **5**, 8332 (2015).

[27] Y. Zhang, S. Krishnamoorthy, F. Akyol, A. A. Allerman, M. W. Moseley, A. M. Armstrong, and S. Rajan, Appl. Phys. Lett. **109**, 121102 (2016).

[28] H. Ahmad, J. Lindemuth, Z. Engel, C. M. Matthews, T. M. McCrone, and W. A. Doolittle, Adv. Mater. **33**, 2104497 (2021).

[29] D. Welch, M. Buonanno, V. Grilj, I. Shuryak, C. Crickmore, A. W. Bigelow, G. Randers-Pehrson, G. W. Johnson, and D. J. Brenner, Sci. Rep. **8**, 2752 (2018).

[30] M. Buonanno, D. Welch, I. Shuryak, and D. J. Brenner, Sci. Rep. **10**, 10285 (2020).

[31] M. Kneissl, T. Seong, J. Han, and H. Amano, Nat. Photon. **13**, 233 (2019).

[32] H. Amano, R. Collazo, C. D. Santi, S. Einfeldt, M. Funato, J. Glaab, S. Hagedorn, A. Hirano, H. Hirayama, R. Ishii, Y. Kashima, Y. Kawakami, R. Kirste, M. Kneissl, R. Martin, F. Mehnke, M. Meneghini, A. Ougazzaden, P. J. Parbrook, S. Rajan *et al.*, J. Phys. D: Appl. Phys. **53**, 503001 (2020).

[33] C. A. Klein, J. Appl. Phys. **39**, 2029 (1968).

[34] N. Nepal, M. L. Nakarmi, K. B. Nam, J. Y. Lin, and H. X. Jiang, Appl. Phys. Lett. **85**, 2271 (2004).

[35] J. R. Haynes, Phys. Rev. Lett. **4**, 361 (1960).

[36] K. B. Nam, M. L. Nakarmi, J. Li, J. Y. Lin, and H. X. Jiang, Appl. Phys. Lett. **83**, 878 (2003).

[37] F. Mireles and S. E. Ulloa, Phys. Rev. B **58**, 3879 (1998).

[38] Y. Zhang, W. Liu, and H. Niu, Phys. Rev. B **77**, 035201 (2008).

[39] Á. Szabó, N. T. Son, E. Janzén, and A. Gali, Appl. Phys. Lett. **96**, 192110 (2010).

[40] J. L. Lyons, A. Janotti, and C. G. Van de Walle, Phys. Rev. Lett. **108**, 156403 (2012).

[41] R. Ishii, A. Kaneta, M. Funato, Y. Kawakami, and A. A. Yamaguchi, Phys. Rev. B **81**, 155202 (2010).

[42] R. Ishii, A. Kaneta, M. Funato, and Y. Kawakami, Phys. Rev. B **87**, 235201 (2013).

[43] M. Funato, K. Matsuda, R. G. Banal, R. Ishii, and Y. Kawakami, Appl. Phys. Express **5**, 082001 (2012).

[44] R. Ishii, M. Funato, and Y. Kawakami, Phys. Rev. B **87**, 161204(R) (2013).

[45] R. Ishii, M. Funato, and Y. Kawakami, Jpn. J. Appl. Phys. **53**, 091001 (2014).

[46] R. Ishii, M. Funato, and Y. Kawakami, Phys. Rev. B **102**, 155202 (2020).

[47] R. Ishii, T. Nagashima, R. Yamamoto, T. Hitomi, M. Funato, and Y. Kawakami, Phys. Rev. B **105**, 205206 (2022).

[48] B. Neuschl, K. Thonke, M. Feneberg, S. Mita, J. Xie, R. Dalmau, R. Collazo, and Z. Sitar, Phys. Status Solidi B **249**, 511 (2012).

[49] R. Ishii, A. Yoshikawa, H. Kobayashi, M. Funato, and Y. Kawakami, Jpn. J. Appl. Phys. **60**, 080901 (2021).

[50] I. Pelant and J. Valenta, *Luminescence Spectroscopy of Semiconductors* (Oxford University Press, New York, 2012).

[51] M. A. Reshchikov and H. Morkoç, J. Appl. Phys. **97**, 061301 (2005).

[52] D. G. Chtchekine, Z. C. Feng, G. D. Gilliland, S. J. Chua, and D. Wolford, Phys. Rev. B **60**, 15980 (1999).

[53] C. Klingshirn, *Semiconductor Optics*, 2nd ed. (Springer, Berlin, 2005).

[54] B. Stébé and G. Munschy, Solid State Commun. **35**, 557 (1980).

[55] I. Vurgaftman and J. R. Meyer, J. Appl. Phys. **94**, 3675 (2003).

[56] Q. Yan, P. Rinke, M. Winkelnkemper, A. Qteish, D. Bimberg, M. Scheffler, and C. G. Van de Walle, Semicond. Sci. Technol. **26**, 014037 (2011).

[57] B. K. Meyer, J. Sann, S. Lautenschläger, M. R. Wagner, and A. Hoffmann, Phys. Rev. B **76**, 184120 (2007).

[58] S. Adachi, J. Appl. Phys. **58**, R1 (1985).

[59] B. Monemar, P. P. Paskov, G. Pozina, C. Hemmingsson, J. P. Bergman, T. Kawashima, H. Amano, I. Akasaki, T. Paskova, S. Figge, D. Hommel, and A. Usui, Phys. Rev. Lett. **102**, 235501 (2009).

[60] Y. Makita, Mater. Sci. Eng. **16**, 265 (1996).

[61] K. Ohkawa and T. Mitsuyu, J. Appl. Phys. **70**, 439 (1991).

[62] Y. Zhang, W. Liu, B. J. Skromme, H. Cheng, S. M. Shibli, and M. C. Tamargo, J. Cryst. Growth **138**, 310 (1994).

[63] C. H. Henry, K. Nassau, and J. W. Shiever, Phys. Rev. B **4**, 2453 (1971).

[64] T. H. Keil, Phys. Rev. **140**, A601 (1965).

[65] B. Monemar, P. P. Paskov, G. Pozina, C. Hemmingsson, J. P. Bergman, S. Khromov, V. N. Izyumskaya, V. Avrutin, X. Li, H. Morkoç, H. Amano, M. Iwaya, and I. Akasaki, J. Appl. Phys. **115**, 053507 (2014).

[66] M. A. Reshchikov, P. Ghimire, and D. O. Demchenko, Phys. Rev. B **97**, 205204 (2018).

[67] D. O. Demchenko, I. C. Diallo, and M. A. Reshchikov, Phys. Rev. B **97**, 205205 (2018).

[68] A. Alkauskas, M. D. McCluskey, and C. G. Van de Walle, J. Appl. Phys. **119**, 181101 (2016).

[69] M. A. Reshchikov, D. O. Demchenko, J. D. McNamara, S. Fernández-Garrido, and R. Calarco, Phys. Rev. B **90**, 035207 (2014).

[70] T. Ogino and M. Aoki, Jpn. J. Appl. Phys. **19**, 2395 (1980).

[71] M. A. Reshchikov, F. Shahedipour, R. Y. Korotkov, M. P. Ulmer, and B. W. Wessels, Phys. B: Condens. Matter **273-274**, 105 (1999).

[72] J. Y. Lyons, A. Alkauskas, A. Janotti, and C. G. Van de Walle, Phys. Status Solidi B **252**, 900 (2015).

[73] P. Giannozzi, S. Baroni, N. Bonini, M. Calandra, R. Car, C. Cavazzoni, D. Ceresoli, G. L. Chiarotti, M. Cococcioni, I. Dabo, A. D. Corso, S. D. Gironcoli, S. Fabris, G. Fratesi, R. Gebauer, U. Gerstmann, C. Gougoussis, A. Kokalj, M. Lazzeri, L. Martin-Samos *et al.*, J. Phys.: Condens. Matter **21**, 395502 (2009).

[74] P. Giannozzi, O. Andreussi, T. Brumme, O. Bunau, M. B. Nardelli, M. Calandra, R. Car, C. Cavazzoni, D. Ceresoli, M. Cococcioni, N. Colonna, I. Carnimeo, A. D. Corso, S. de Gironcoli, P. Delugas, R. A. DiStasio Jr., A. Ferretti, A. Floris, G. Fratesi, G. Fugallo, R. Gebauer *et al.*, J. Phys.: Condens. Matter **29**, 465901 (2017).

[75] M. A. Moram and M. E. Vickers, Rep. Prog. Phys. **72**, 036502 (2009).

[76] S. P. Ong, W. D. Richards, A. Jain, G. Hautier, M. Kocher, S. Cholia, D. Gunter, V. L. Chevrier, K. A. Persson, G. Ceder, Comput. Mater. Sci. **68**, 314 (2013).

[77] K. Momma and F. Izumi, J. Appl. Crystallogr. **44**, 1272 (2011).

[78] F. Oba and Y. Kumagai, Appl. Phys. Express **11**, 060101 (2018).

[79] J. A. Déverin, Nuov. Cim. B **63**, 1 (1969).

[80] R. W. Keyes, IBM J. Res. Dev. **5**, 65 (1961).

[81] M. Feneberg, M. F. Romero, M. Röppischer, C. Cobet, N. Esser, B. Neuschl, K. Thonke, M. Bickermann, and R. Goldhahn, Phys. Rev. B **87**, 235209 (2013).

[82] K. Kim, W. R. L. Lambrecht, B. Segall, and M. van Schilfgaarde, Phys. Rev. B **56**, 7363 (1997).

[83] A. Punya and W. R. L. Lambrecht, Phys. Rev. B **85**, 195147 (2012).

[84] H. Sezen, H. Shang, F. Bebensee, C. Yang, M. Buchholz, A. Nefedov, S. Heissler, C. Carbogno, M. Scheffler, P. Rinke, and C. Wöll, Nat. Commun. **6**, 6901 (2015).

[85] Y. Yamada, H. Mino, T. Kawahara, K. Oto, H. Suzuura, and Y. Kanemitsu, Phys. Rev. Lett. **126**, 237401 (2021).

[86] S. T. Pantelides, Rev. Mod. Phys. **50**, 797 (1978).

[87] C. H. Park and D. J. Chadi, Phys. Rev. B **55**, 12995 (1997).

[88] S. Lany and A. Zunger, Appl. Phys. Lett. **96**, 142114 (2010).

[89] M. H. Breckenridge, Q. Guo, A. Klump, B. Sarkar, Y. Guan, J. Tweedie, R. Kirste, S. Mita, P. Reddy, R. Collazo, and Z. Sitar, Appl. Phys. Lett. **116**, 172103 (2020).

[90] M. H. Breckenridge, P. Bagheri, Q. Guo, B. Sarkar, D. Khachariya, S. Pavlidis, J. Tweedie, R. Kirste, S. Mita, P. Reddy, R. Collazo, and Z. Sitar, Appl. Phys. Lett. **118**, 112104 (2021).